ECS Transactions, 78 (1) 783-793 (2017)
10.1149/07801.0783ecst ©The Electrochemical Society

Effect of Surfactants on the Physico-Chemical Characteristics of $IrO/Ce_{0.8}Sm_{0.2}O_{2-\delta}$ Nanocomposite for SOFC Application

Chima B.Njoku[a], Bernard Omondi[b] , and Patrick G. Ndungu[c]

[a b, c]School of Chemistry and Physics, Westville Campus, University of KwaZulu-Natal Private Bag X 54001, Durban 4000, South Africa
[c] Department of Applied Chemistry, Doornfontein Campus, University of Johannesburg, P.O. Box 17011, Doornfontein 2028, Johannesburg, South Africa.

Sol-gel technique takes advantage of the structural directing properties and templating characteristics of non-ionic, anionic and cationic surfactant to produce porous Iridium oxide, with Samarium doped Ceria (SDC) nanoparticles. The nano-powders were calcined at a temperature of 950°C, and the crystalline nano-structures and compositions were characterized by high resolution transmission electron microscopy and X-ray diffraction. Textural characteristics and particle morphology were respectively characterized by Nitrogen sorption at 77.5 K and scanning electron microscopy. The nature of the surfactant influenced particle morphology, pore diameter, pore size, Crystallite size, surface area and electrochemical properties.

Introduction

Sol-gel synthesis is a promising method to produce oxide ceramic materials, with controlled structure and composition for many applications (1-3). This method is simple cost-effective, high yielding final product and has a low reaction temperature (3,4). It is an efficient way to prepare samarium doped ceria nanoparticles with Iridium oxide (5), because it synthesizes monodispersed particles, with controllable sizes in the nanometer scale. This method also regulates particle interactions at certain stages of material formation, and is necessary for the perfect structure of material (6).

The surfactant-assistant technique thus is suitable to provide materials with appropriate pore diameter, high surface areas and a better access to active sites (7-9). The surfactants nature influences particle morphology as no simple selection rule can be applied to predict which surfactant will give a particular particle size. Their structures, stabilization of the micelle walls and reduced inter-droplet exchange, produces smaller particles, crystals, and prevents metallic nanoparticles aggregation into matrices (10).

The surfactants used in these methods are Pluronic P123 block copolymer, Pluronic F-127 block copolymer (11-14), Sodium dodecyl sulfate (SDS), Cetyl trimethyl ammonium bromide (CTAB) and Polyethylene glycol (PEG). The materials formed were used in low temperature solid oxide fuel cells application.

Materials and Method

Synthesis of Nanocrystalline Materials

The starting material: Cerium (III) acetyl acetonate hydrate, $Ce(acac)_3$, ($C_{15}H_{21}CeO_{6-x}H_2O$), (99.9 % purity) and Samarium (III) acetyl acetonate hydrate, ($C_{15}H_{21}SmO_{6-x}H_2O$), (99.9 %), was purchased from Aldrich chemicals USA. Surfactants, Pluronic F-127 powder (bioreagent, suitable for cell culture), Polyethylene glycol (PEG), Pluronic P123 (P123), Sodium dodecyl sulphate (SDS) and Cetyl triammonium bromide (CTAB) were purchased from sigma Life Science Germany. Iridium (III) acetylacetonate was purchased from Industrial Analytical Chemicals pty South Africa. These chemical reagents were used as acquired from their commercial sources without further purification.

Preparation of IrO-$Ce_{0.8}Sm_{0.2}O_{2-\delta}$

The materials and mass used are 0.720 g of Cerium acac $Ce(acac)_3$ and 0.200 g of Samarium acac $Sm(acac)_3$ and 0.022 g of Iridium $(acac)_3$ and 5 wt % of the surfactants (2.500 g). These were added to 40 ml of ethanol and 10 ml of deionized water as solvents and the mixture was sonicated for 30 mins. The mixture was stirred on a hot plate for 30 mins at a temperature of 80°C, to form a sol. The hydrolysis, condensation, solvent evaporation occurred rapidly and a collapse of the gel network. The sol was dried in an oven for 18hrs and calcined with a Kittec Squadro furnace for 4hrs at 950°C. This method was applied to all the surfactants.

Preparation of IrO-$Ce_{0.8}Sm_{0.2}O_{2-\delta}$ without Surfactant

The materials and mass used are 0.720 g of Cerium $(acac)_3$, 0.200 g of Samarium $(acac)_3$ and 0.022 g of Iridium $(acac)_3$. These were added to 40 ml of ethanol and 10 ml of deionized water as solvents and the mixture was sonicated for 30 mins. The mixture was stirred on hot plate for 2 hrs at a temperature of 80°C. The hydrolysis, condensation and solvent evaporation was sluggish .The sample was dried in an oven for 18hrs and calcined with a kittec squadro furnace for 4 hrs at 950°C. The summary and synthesis processes are shown in table I.

Table I: The summary and processes used for synthesis conditions.

Sample ID	Mass of sample (5wt %)	Surfactant Name	Type
F-127	5 wt%	Pluronic F-127	Non-IONIC
P123	5 wt%	Pluronic P123	Non-IONIC
PEG	5 wt%	PolyethyleneGlycol	Non-IONIC
SDS	5 wt%	SodiumDodecylSulphate	ANIONIC
CTAB	5 wt%	CetylTriammoniumBromide	CATIONIC
WS	Not added	No Surfactant	–

Characterization

The crystal structure, crystal size, lattice spacing and the phase present in the powder were analyzed with X-ray diffraction (XRD). This instrument (Phillips PW3710)

works with voltage and current settings of 30 kV and 35 mA, respectively and uses Cu-Kα radiation (1.5405 Å) for qualitative analysis, the XRD diffractogram were recorded between the intervals of 5° ≤ 2θ ≤ 90° at a scan speed of 2 °/min. The mean crystallite sizes 'D' were determined according to the Scherer equation (15):

$$D = 0.9\lambda/\beta cos\theta \quad (1)$$

Where; λ = X-ray wavelength (1.5405 Å), β = full width at half maximum of the diffraction line, and θ = diffraction angle.

.

Fourier Transform Infrared Spectroscopy (FT-IR) performed the functional group analysis. The lattice fringes and diffraction patterns were carried out by the high-resolution transmission electron microscopy (HR-TEM). Scanning electron microscopy (SEM X130) was used to characterize the morphology and grain size of the powder. The samples were coated with gold before the examination. N_2 adsorption- desorption, was done using the Tri-Star II3020 V1.03 to find the surface area, pore size, pore volume, and the pore size distribution. The samples were degassed using the degassing instrument at 90°C for 1 hr and then was raised to 200°C and it remained at the temperature for 5 hrs. The samples were put in a Tristar II3020 V1.03 using Nitrogen at 77 k, to carry out this process.

Electrochemical Performance Test

To analyse the electrochemical properties, the electrolyte disc was sandwiched between the anode and cathode discs, and then placed in the open flange test set-up from Fiaxell SOFC Technologies™. This set-up was designed for the cell sizes, and platinum meshes were used as contact components, to act as combined current collector and gas distributor. The test-bed was placed in a Kittec Squadro muffle furnace and linked to appropriate gas tight fittings for the delivery of humidified air and hydrogen (~ 4-20 % water) gas to the cell. The wire of the mesh was connected to a Nuvant™ Powerstat 05 potentiostat and galvanostat where the current and voltage from the cells were measured. Polarization curves were recorded between 300 - 500 °C. The ionic conductivity was calculated thus (15).

$$\sigma = \frac{l}{RS} \quad (2)$$

where, *l* is the electrolyte thickness, S is electrode area of the electrolyte surface and R is resistance in ohms (cell resistance).The activation energy was calculated using it in the Arrhenius plot (15).

$$\sigma = \sigma^o \exp\left[\frac{E_a}{kT}\right] \quad (3)$$

Where E_a is the activation energy of conduction, T is the absolute temperature, σ_o is the pre-exponential factor and k is the Boltzmann Constant.

Results and Discussion

FTIR Analysis

Figure 1 shows the Infrared Spectroscopy that was used to investigate the functionalization and vibrational modes of IrO-$Ce_{0.8}Sm_{0.2}O_{2-\alpha}$ composites materials

formed from surfactant assisted sol gel method and calcined at 950 °C. The surfactants used were PEG, SDS, F127, P123 and CTAB. At the calcination temperature, the surfactants were burnt off, leaving just the metal composite.

From figure 1 the addition of surfactants showed an evidence of shifts in the peaks observed from the spectra. For F127, the perovskite metals showed absorbance peaks at 476.06 cm^{-1} which are suspected to be peaks of iridium oxide and 1026.51cm^{-1} which are strong C-O bond of ethers which are bonded to the SDC metal as shown in the figure 1 .The spectra for P123 showed absorbance peaks at 1562.95 cm^{-1} show a strong C-O bond which are absorbance for samarium doped ceria (16), and it stretches to a strong broad bond of a O-H phenol hydrogen bonded group of the adsorbed water from the hydrates at 3421.10 cm^{-1}. The perovskite metal formed for PEG surfactant showed absorbance peaks at 1562.95 cm^{-1} and peaks at 3421.10 cm^{-1} also. The sample that had CTAB added to it showed absorbance peaks at 471.86 cm^{-1}, 1054.82 cm^{-1} and 3163.58 cm^{-1}. The samples with SDS added to it show absorbance peaks at 589.63cm^{-1}, 610.96 cm^{-1},635.10 cm^{-1} and 992.03 cm^{-1} that are peaks that were formed in the finger print region which confirmed metal peaks. The sample without the surfactants showed absorbance peaks at 528.90 cm^{-1}, 926.67 cm^{-1}, 1017.54 cm^{-1}, 1258.47 cm^{-1}, 1375.10 cm^{-1}, 1513.09 cm^{-1}, 1579.09 cm^{-1} and 3151.99 cm^{-1}.

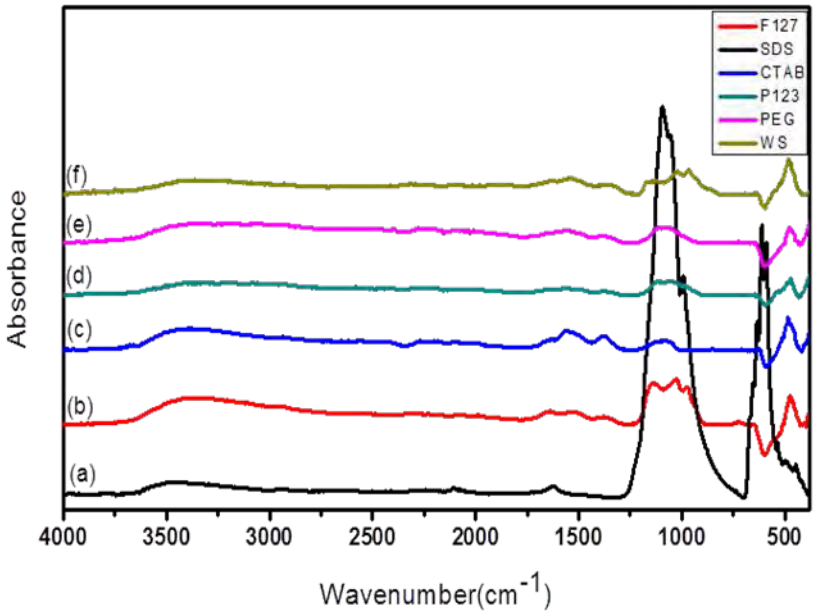

Figure 1. Shows the FTIR spectra of F127, SDS, CTAB, P123, PEG and WS, surfactants added to IrO/$Ce_{0.8}Sm_{0.2}O_{2-\delta}$ calcined at 950°C.

Research has shown that acacH consists of keto and enol tautomers. The replacement of the enolic hydrogen atom of acacH by a metal cation, as shown in figure 2, produces a six membered metallocycle, thereby shifting the keto–enol equilibrium in favor of the chelated enolate anion formed in metal acetylacetonate complexes. The chelation of the acac ligands to transition metal ions will result in displacement of the carbonyl-stretching bond of the acac group. Many researchers with many transition metals have observed this phenomenon, although the extent of shifting is different for different transition metals (16-18), in all cases the characteristic absorbance of the metals shift to the lower frequency regions, similar to what was observed in this study (16).

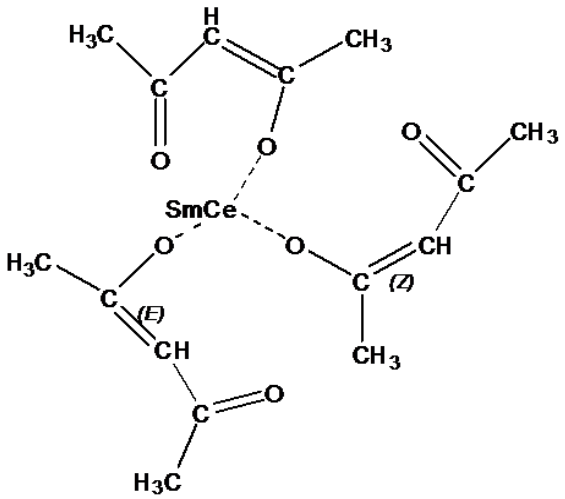

Figure 2. Schematic of the chelation of the acac ligands to transition metal ions.

Powder XRD Analysis

Figure 3 confirms the structural phase of Cerium and Samarium (CeO_2) peaks and IrO_2 peaks, for all surfactants. The diffractogram displayed the same structural pattern, except for the SDS surfactant, where the structure was not totally formed. The structural pattern decreased in peak intensity from left to right as the angle 2θ increased, with very sharp peaks. The X-ray diffraction peaks were located at 2 theta values of 28.50°, 34.67°, 40.12°, 47.19°, 53.92°, 58.63°, 65.89°, 69.17°, 76.25°, 78.61°, 83.32° and 87.87° which are indexed to (111), (101), (200), (220), (211), (002), (310), (301), (331), (420), (321) and (422) respectively.

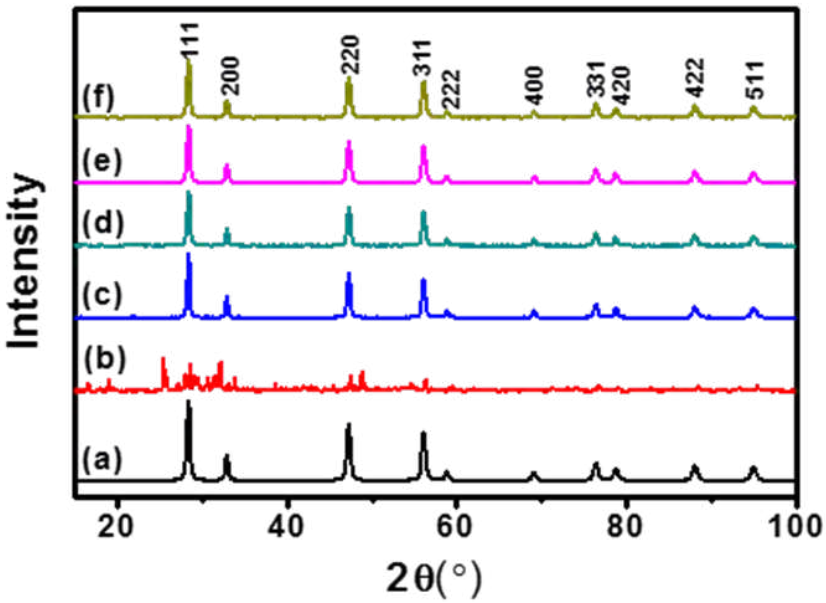

Figure 3. X-ray Diffraction pattern of (a) F127 (b) SDS (c) PEG (d) P123 (e) CTAB (f) WS, surfactants added to IrO/$Ce_{0.8}Sm_{0.2}O_{2-\delta}$ and calcined at 950°C.

The average crystallite sizes are 30.96 nm for F-127, 32.96 nm for P123, 36.66 nm for PEG, 43.11 nm for CTAB, 98.61 nm for SDS, and 34.06 nm for WS. The crystallite sizes were calculated from the Scherer equation, using the most crystalline

peak and the values are shown in Table II. These confirmed that the surfactants affect the crystalline nature of the samples, this also corresponds with the particle sizes from the HRTEM images, confirming the lateral relationship between the particle sizes of the sample and its crystallite size, showing confirmation of the surfactants effect.

HRTEM Analysis

Figure 4 shows the HRTEM analysis of the low magnification, lattice fringes and diffraction patterns of the perovskite, which depicts the effects of surfactants on the sample. The low magnification of the image revealed the particles sizes and their formation. The change, in the particle shapes and sizes are evidences, of the effect of surfactant on the materials. The sample particle sizes were in the range of 2.63 - 30.49 nm for P123, 3.55 - 30.38 nm for F127, 1.82 - 67.96 nm for CTAB; 2.73 -51.997 nm for PEG, 1.73 -79.596 nm for SDS, and 3.420 - 66.56 nm for WS.

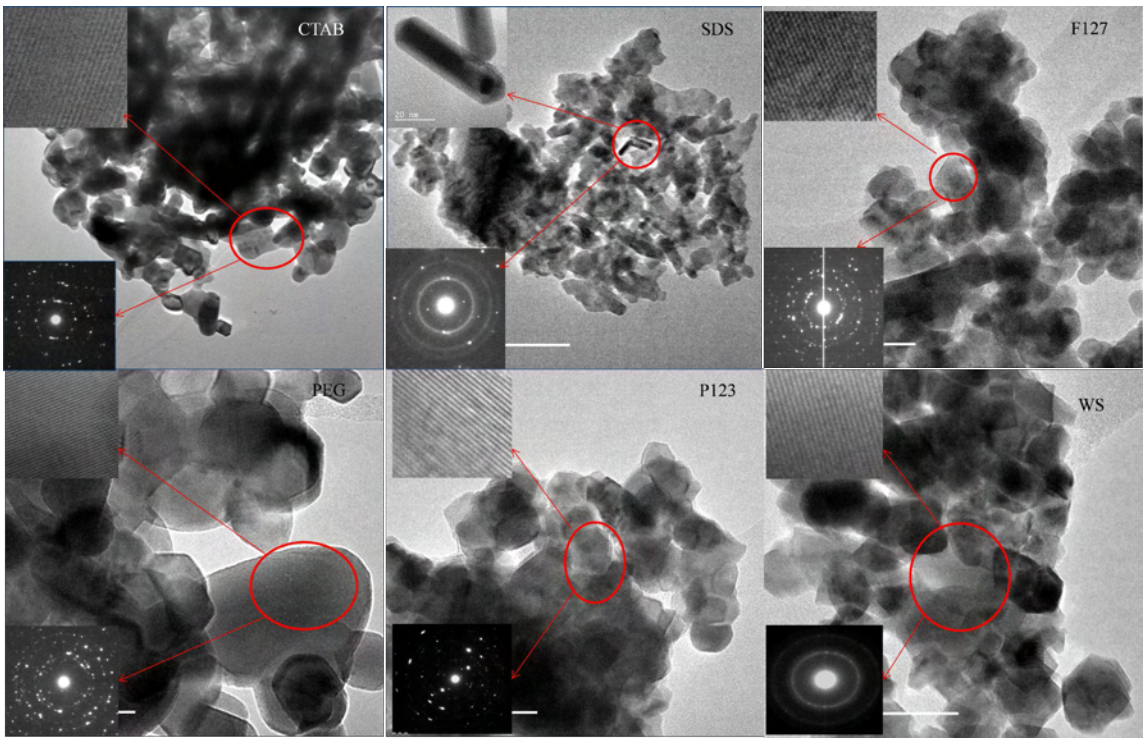

Figure 4. The Low magnification, Lattice fringes and diffraction patterns of (a) F12 (b) SDS(c) CTAB (d) PEG (e) P123 (f) WS, surfactants added to IrO/$Ce_{0.8}Sm_{0.2}O_{2-\delta}$ and Calcined at 950°C.

The XRD diffractogram corresponds with the varying particle sizes by displaying similar crystallite sizes. The lattice fringes also showed varying distances between the crystal layers, 0.142 (310) for P123, 0.124 (331) for F127, 0.152 (311) for CTAB 0.126 (321) for PEG. 0.181 (400) for WS; and the particles for SDS were rectangular. The value in brackets is the Miller's index for the crystal layer distance.

SEM Analysis

The Morphology of P123 surfactant on IrO-$Ce_{0.8}Sm_{0.2}O_{2-\delta}$, showed in Figure 5a, fine particles held together by strong and weak bonds between the metal combinations to

form agglomerates. F-127 surfactant in Figure 5b revealed that the metals were accumulated in agglomerate formation with large pore sizes. In Figure 5c, the effect of CTAB, displayed an agglomerate of fine particles with pore spaces between them. The morphology of PEG effects revealed a gel like structure with smooth surfaces separated by pores as shown in Figure 5d. Figure 5e showed the effect of SDS on the sample, the morphology revealed large smooth aggregate surfaces with smaller loose particles.

The image showing the nanoparticles prepared without surfactants, revealed tiny particle separations to form bigger loosely packed particles, these particles bond and grew asymmetrically to form agglomerates as shown in figure 5f. The addition of surfactants produces particle separation and formation of loosely coherent secondary particles called agglomerates. Finely divided porous solids were also formed by this method and are distinguished by large surface to volume ratios, enhanced chemical reactivity and high adsorption capacity.

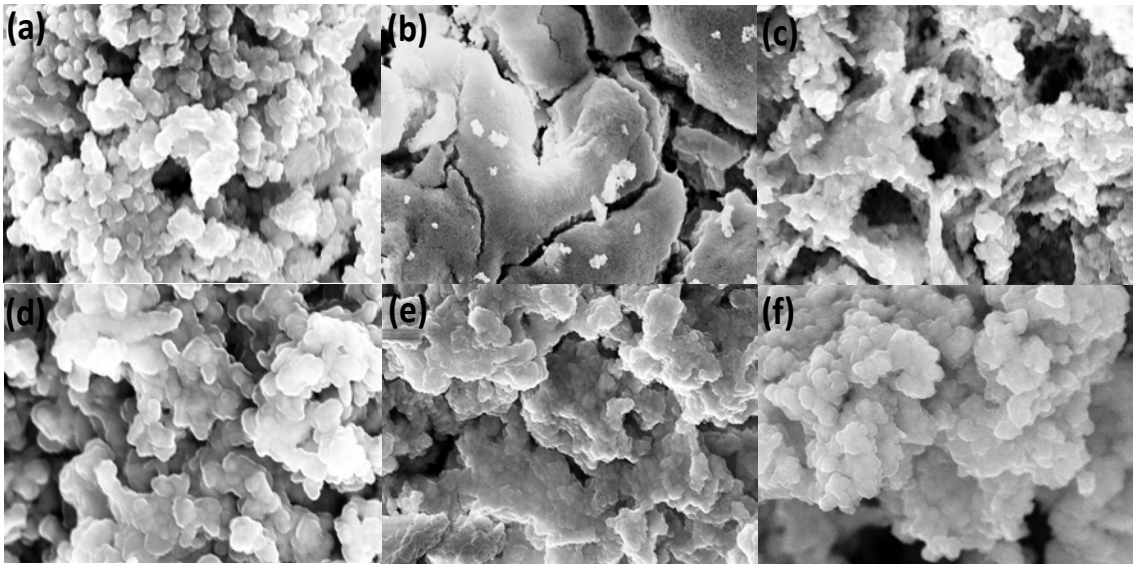

Figure 5. SEM morphology of (a) CTAB (b) SDS (c) F-127 (d) P123 (e) WS and (f) PEG added to IrO/$Ce_{0.8}Sm_{0.2}O_{2-\delta}$ and calcined at 950°C.

BET Analysis

The isotherm plot in figure 6 confirmed the samples are macro porous materials, because the isotherm plots were type II. The surface area of F-127 prepared material, in comparison with the others, produced the highest surface area as shown in the Table II. The addition of surfactant increases or lowers the surface area, and affects particles sizes of materials as shown by the analysis in the table. The same effects are seen in HRTEM and XRD Crystallite sizes. Pore sizes of the material also varied as shown by the analysis and confirmed by SEM analysis.

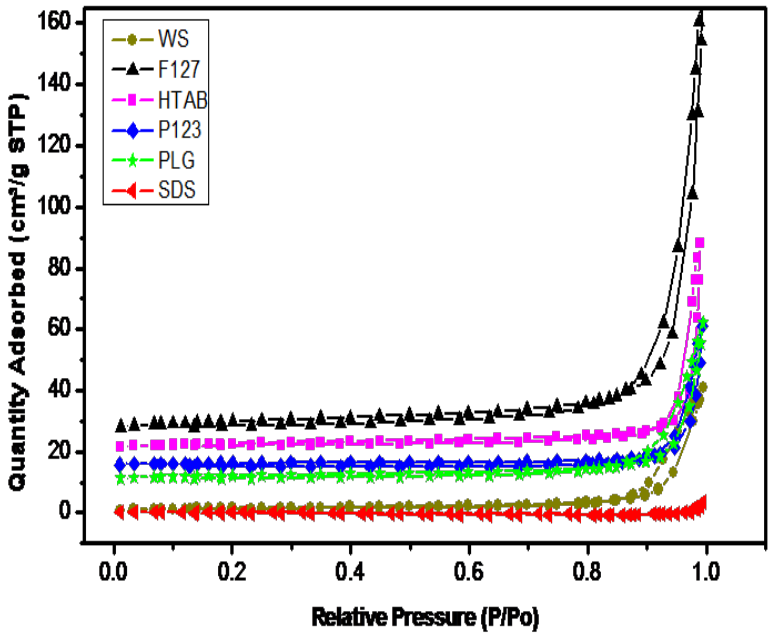

Figure 6. Isotherm plots for (a) WS (b) F127 (c) CTAB (d) P123 (e) PEG and (f) SDS added to IrO/$Ce_{0.8}Sm_{0.2}O_2$ and calcined at 950°C.

Table II: The Surface Area, Pore diameter, Pore volume and Crystallite size of (a) F127 (b) CTAB (c) PEG (d) WS (e) P123 and (f) SDS, added to IrO/$Ce_{0.8}Sm_{0.2}O_2$ and calcined at 950 °C.

Sample ID	Surface area (m^2/g)	Pore diameter (nm)	Pore volume (cm^3/g)	Crystallite size (nm)
F127	17.514	37.5	0.1641	33.87
CTAB	9.7064	27.8	0.0678	46.65
PEG	7.6359	29.5	0.0546	39.61
WS	5.5301	39.9	0.0552	43.85
P123	4.4621	32.5	0.0363	35.64
SDS	1.2478	18.58	0.0111	98.61

Electrochemical Properties

Polarization. The polarization curves for IrO/SDC synthesized with different surfactants are shown in Figure 7. These were obtained using humidified hydrogen and compressed air at temperature intervals of 300°C-500°C. At the cell temperature of 500°C the current density was lower than the current density of 300°C-400°C but generated a higher power density because of its low polarization losses and anodic overvoltage as shown in the graph. The ohmic overpotential decreased, when the cell testing temperature increased from 300 - 500°C, corroborating a high resistance at lower temperature that lowers the power. The concentration overpotential are losses observed when current flows through the cell. This is more pronounced when fuel or oxidant gases with low purities are fed in to the cell. The OCV values of the tested cells, as shown in Figure 5, which decreased when measured from 300-500°C and were stable at 1.1 V for more than 15 hours at 500°C for all calcined samples.

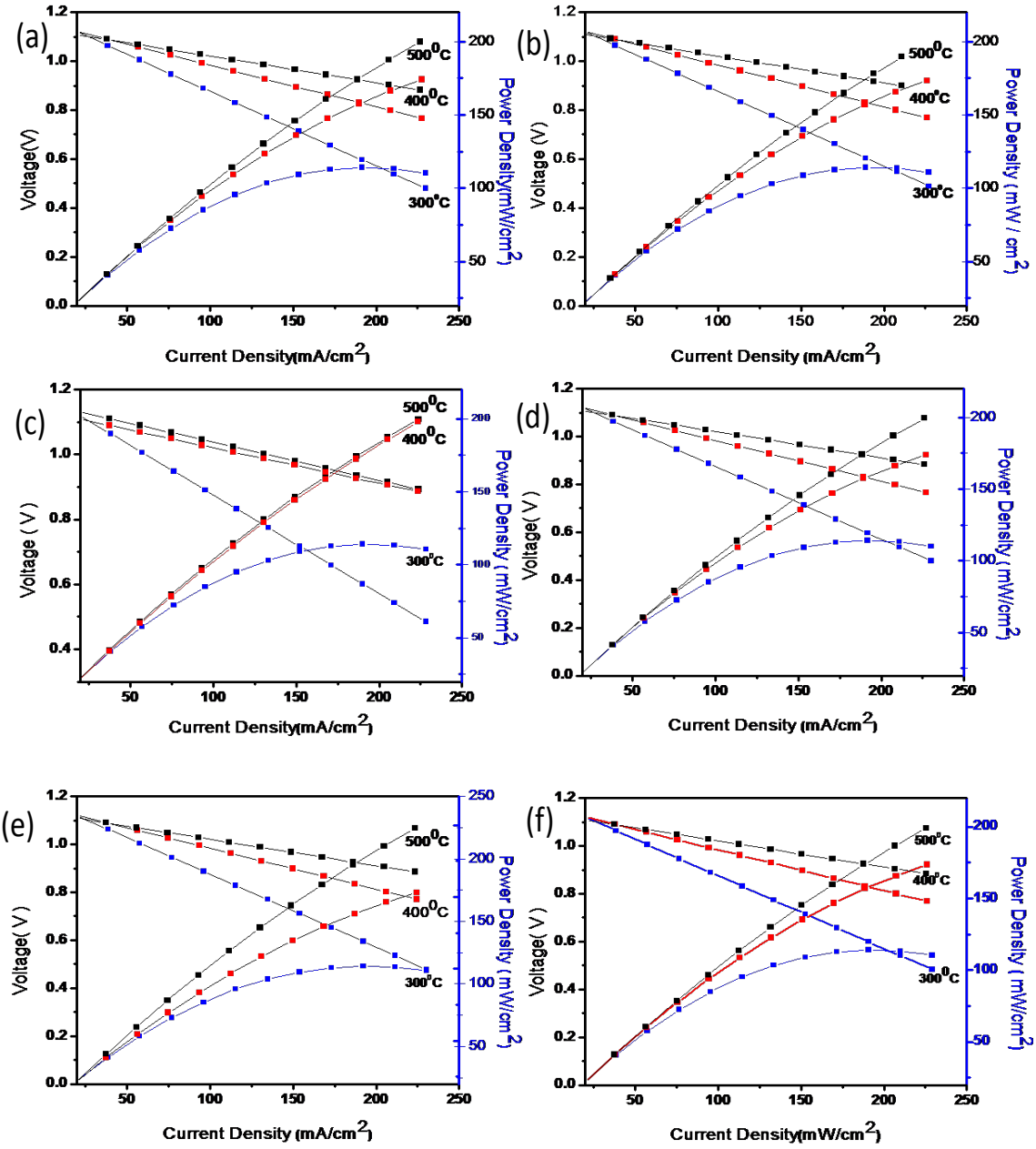

Figure 7. The polarization curve of (a) WS (b) F-127 (c) CTAB (d) P123 (e) PEG (f) SDS added to IrO/$Ce_{0.8}Sm_{0.2}O_{2-\delta}$ and calcined at 950°C.

This value is lower than the thermodynamic values calculated using the Nernst equation, which could be attributed to the assembly and structure of the cell and gas crossing through the electrolyte could account for the lower OCV.

Power Density. Figure 8 shows the power densities of the different samples, which extends from 300°C-500°C. The maximum power densities were recorded at 500°C with a maximum value of 199 mW/cm^2 obtained from the samples synthesized with F-127, CTAB and PEG.

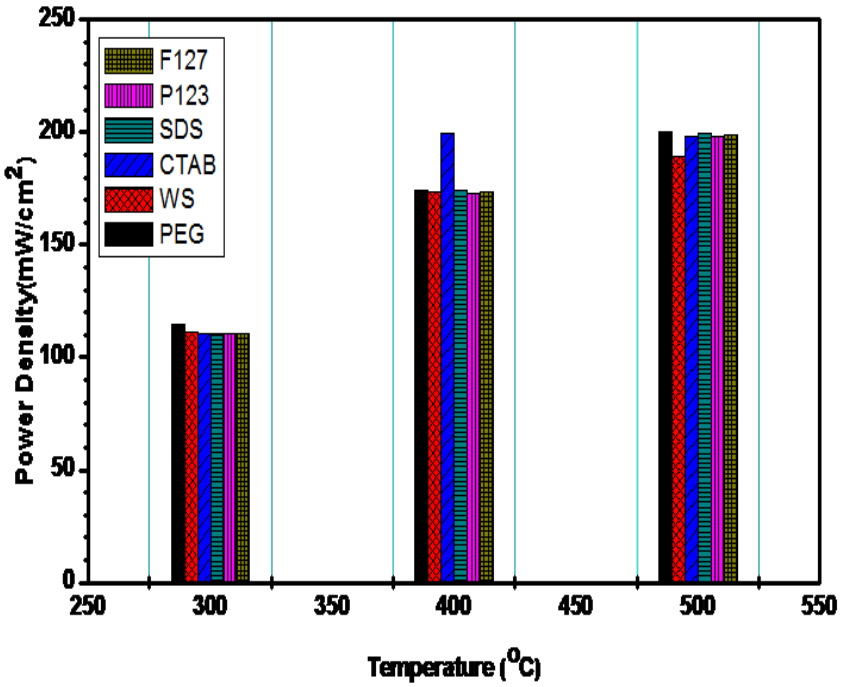

Figure 8. The Power Density graph of (a) F127 (b) P123 (c). SDS (d).CTAB (e).WS and (f).PEG added to IrO/$Ce_{0.8}Sm_{0.2}O_{2-\delta}$ and calcined at 950°C.

Conclusion

The nature of the surfactant influenced particle morphology, pore diameter, pore size, crystallite size, surface area and electrochemical properties. Surfactants addition caused a reduction in the crystallite sizes. This reduction was caused by an increase in the XRD peak intensities and a high, full width at half maximum value. Increase in the materials surface area was influenced by F127, CTAB, PEG and reduced by SDS and P123 compared with the sample without surfactant. The materials morphology changed from surfactant to surfactant with varying porosity and particle sizes, resulting from a complete coalescing of the substituent materials. The materials were tested as anodes and the electrochemical properties were obtained. These properties include the power density, current density and polarization resistance. The results obtained for F-127 surfactant displayed the highest power density of 199 mW/cm^2, a current density of 226 mA/cm^2 and low polarization resistance of 0.981 Ω cm^2. It was revealed that Nonionic and cationic surfactants showed good qualities for our material, because of its surface area, low crystallite size, porous morphology and low polarization resistance. This research also revealed that surfactants are essential for material boosting and increased electrical performance in solid oxide fuel cell application.

Acknowledgement

The authors thank the University of KwaZulu-Natal, Westville campus for availability to research facilities used in this research.

References

1. S. J. Kalita, B. Abhilasha, and A. B. Himesh, *Mater. Sci. Eng.,* **27,** 441-449 (2007) .
2. Z. Lou, J.Peng, N. Dai, J.Qiao, Y. Yan, Z.Wang, J. Wang, K. Sun, *Electrochem. Commun.,* **22,** 97–100 (2012).
3. M. S. Mastuli, N. S. Ansaria, M. A. Nawawia, A. Maria, *APCBEE Procedia.,* **3**, 93 – 98 (2012).
4. Z. Lou, J. Qiao, Y. Yan, J. Peng, Z. Wang, T. Jiang, K. Sun, *Electrochem. Commun.,* **37**, 11345-11350 (2012).
5. N. I. Ermokhina, V. A. Nevinsky, P. A. Manorik, V. G. Ilyin, N. N. Shcherbatyuk, D. O. Klymchuk, A. M. Puziy, *Mater. Lett.*, **75**, 68–70, (2012).
6. K. T. Parada, G. V. Aguilar, A. Mantilla, M. A. Valenzuela, E. Hernández, *Fuel ,* **110**, 70 –75 (2013).
7. L. F. Chen, J. A. Wang, L. E. Norena, J. Aguilar, J. Navarrete, O. Salas, *J Solid State Chem.,* **180**, 2958–2972 (2007).
8. O. A. Gonzalez, M. A. Valenzuela, J. A. Wang, *MRS,* **885**, 223–238 (2006).
9. P. Schacht, S. Ramirez, J. Ancheyta, *Energy Fuels,* **23**, 4860 – 4865 (2009).
10. S. K. Das, M. K. Bhunia, A. K. Sinha, A. Bhaumik, *J. Phys.Chem.,* **113**, 8918–8923 (2009).
11. S. G. Liu, H. Wang, J. P. Li, N. Zhao, W. Wei, Y. H. Sun, *Mater. Res. Bull.,* **42**, 171–176 (2007).
12. K. Wang, M. A. Morris, J. D. Holmes, J. Yu, R. Xu, *Micropor. Mesopor. Mater.*,**117**, 161–164 (2009).
13. G. Duan, C. A. Zhang, X. Li, L. Yang, X. Lu, *Nanoscale Res. Lett.*, **3**,118–122 (2008).
14. Y. Chen, S. K. Lunsford, Y. Song, H. Ju, P. Falaras, V. likodimos, A.G. Kontos, D. D. Dionysiu, *Chem. Eng. J.,* **170**, 518–524 (2011).
15. C. B. Njoku, P. G. Ndungu, *J. Nano Res.,* **44**, 35-50 (2016).
16. P. Blennow, J. Hjelm, T. Klemens, S. Ramousse, A. Kromp, A. Leonide, A. Weber, *J. Power Sources*, **196,** 7117– 7125 (2011).
17. C. Shen, L. L. Shaw, *J Sol-gel Sci Technol.*, **53**, 571–577 (2010).
18. M. C. Brasil, E. V. Benvenutti, J. R. Gregorio, A. E.Gerbase, *React Funct Polym.,* **63**, 135–141 (2005).